

Si-nanostructures formation in amorphous silicon nitride $\text{SiN}_x\text{:H}$ deposited by remote PECVD

A. Zerga*, M. Carrada, M. Amann, A. Slaoui

Institut d'Electronique du Solide et des Systèmes InESS – CNRS (UMR 7163), 23 rue du Loess, 67037 Strasbourg, France

Available online 17 December 2006

Abstract

The formation of silicon nanoclusters embedded in amorphous silicon nitride ($\text{SiN}_x\text{:H}$) can be of great interest for optoelectronic devices such as solar cells. Here amorphous $\text{SiN}_x\text{:H}$ layers have been deposited by remote microwave-assisted chemical vapor deposition at 300 °C substrate temperature and with different ammonia [NH_3]/silane [SiH_4] gas flow ratios ($R = 0.5\text{--}5$). Post-thermal annealing was carried out at 700 °C during 30 min to form the silicon nanoclusters. The composition of the layers was determined by Rutherford back scattering (RBS) and elastic recoil detection analysis (ERDA). Fourier transform infrared spectroscopy (FTIR) showed that the densities of Si–H (2160 cm^{-1}) and N–H (3330 cm^{-1}) molecules are reduced after thermal annealing for $\text{SiN}_x\text{:H}$ films deposited at flow gas ratio $R > 1.5$. Breaking the Si–H bonding provide Si atoms in excess in the bulk of the layer, which can nucleate and form Si nanostructures. The analysis of the photoluminescence (PL) spectra for different stoichiometric layers showed a strong dependence of the peak characteristics (position, intensity, etc.) on the gas flow ratio. On the other hand, transmission electron microscopy (TEM) analysis proves the presence of silicon nanoclusters embedded in the films deposited at a gas flow ratio of $R = 2$ and annealed at 700 °C (30 min). © 2007 Elsevier B.V. All rights reserved.

PACS: 81.07.–b; 81.15.Gh

Keywords: Nanoclusters; Silicon; $\text{SiN}_x\text{:H}$; Photoluminescence

1. Introduction

Amorphous silicon nitride ($\text{SiN}_x\text{:H}$) films are widely used in the silicon solar cell industry as antireflection coatings, passivation layers, dopant diffusion barriers and recently as spectral response converters [1]. Recently, many researchers have turned their attention to develop this last application for optoelectronic and photonic devices by taking advantage of the spectral response properties of silicon nanoclusters [2,3]. Indeed, the room temperature photoluminescence (PL) of deposited $\text{SiN}_x\text{:H}$ films show the possibility of converting the ultraviolet photons into red ones as a consequence of radiative recombination processes in silicon nanoclusters and defects of the matrix material. Consequently, the quantum efficiency for crystalline silicon solar cells can be increased.

In the literature, several authors have reported that silicon nanoclusters can be synthesized either during the growth of $\text{SiN}_x\text{:H}$ films [4,5] deposited at moderate temperatures or after post-thermal annealing [6,7]. However, their formation is closely related to the deposition conditions (plasma characteristics, temperature, pressure, density and dilution of gases, etc.) and to the thermal annealing process (temperature, ambient, etc.). The use of thermal annealing favors the coalescence of silicon atoms resulting mainly from the breaking of the Si–H and Si–N molecules and also improves the defect passivation at nc-Si/ $\text{SiN}_x\text{:H}$ interfaces due to the released hydrogen atoms.

In this study, we investigated the conditions for the formation of silicon nanoparticles in an amorphous $\text{SiN}_x\text{:H}$ matrix. The $\text{SiN}_x\text{:H}$ films were deposited by remote plasma enhanced chemical vapor deposition (PECVD) at 300 °C with different gas flow ratios of NH_3 and SiH_4 . The CVD technique is well established for the deposition for $\text{SiN}_x\text{:H}$ films. After deposition, the films were annealed at 700 °C for 30 min under a nitrogen atmosphere.

*Corresponding author. Tel.: +33 3 88 10 63 36; fax: +33 3 88 10 63 35.
E-mail address: zerga@iness.c-strasbourg.fr (A. Zerga).

The aim of this work is to show the relationship between the $\text{SiN}_x\text{:H}$ films structural properties, and the conditions of the silicon nanoclusters formation, as well as to understand the mechanisms responsible of the observed room temperature PL.

1.1. Experimental

$\text{SiN}_x\text{:H}$ films were deposited at 300 °C on (100) p-type silicon substrate ($\rho = 1\text{--}10\ \Omega\text{cm}$) by remote PECVD using a mixture of pure silane (SiH_4) and ammonia (NH_3). The gas flow ratio $R([\text{NH}_3]/[\text{SiH}_4])$ was varied between 0.5 and 5 by keeping the SiH_4 flow constant at 14 sccm. The NH_3 is dissociated in the top of the reactor chamber by absorbing microwave power ($f = 2.45\ \text{GHz}$ and $P_{\text{MW}} = 600\ \text{W}$) and the SiH_4 is dissociated in the bottom of the reactor by absorbing radio frequency power ($f = 13.56\ \text{MHz}$ and $P_{\text{rf}} = 250\ \text{W}$). The film precursors formed by chemical reaction in the gaseous phase between the species of NH_3 and SiH_4 were deposited on the polarized and heated substrate ($V_{\text{bias}} = 70\ \text{V}$). The deposition velocity varied from 10 to 20 nm/min depending on the ratio of the gas flow R . After deposition, the $\text{SiN}_x\text{:H}$ films were annealed in a conventional tube furnace under nitrogen atmosphere at 700 °C for 30 min.

The structural properties of the $\text{SiN}_x\text{:H}$ deposited films were investigated by Fourier transform infrared spectroscopy (FTIR) using an Bruker-Equinox 55 spectrophotometer with $2\ \text{cm}^{-1}$ resolution and ($400\text{--}5000\ \text{cm}^{-1}$) wave number domain. The $\text{Si}_{1-x-y}\text{N}_x\text{H}_y$ layer composition was deduced from Rutherford backscattering spectrometry (RBS) and elastic recoil detection analysis (ERDA). The refractive index was determined by ellipsometry using a ‘Gaertner’ ellipsometer with a He–Ne laser at 632.8 nm wavelength, while the thickness was determined from UV–visible reflectance. PL spectra were recorded at room temperature using a 355 nm excitation wavelength of a Nd:YVO₄ laser. The emitted light was detected by a BWTek BCR 112E spectrometer coupled with a Sony ILX511 CCD linear image sensor. Transmission electron microscopy (TEM) observations were performed with a Topcon 002B microscope operating at 200 kV.

2. Results and discussion

2.1. Structural characterizations

One of the necessary conditions for Si nucleation is to deposit a Si-rich $\text{SiN}_x\text{:H}$ matrix, with $x > 1.33$, stoichiometric composition being $\text{Si}_3\text{N}_4\text{:H}$. Moreover, several authors have shown that nitrogen N has a crucial role in the formation of nucleation sites; in particular a high concentration in the gas flow of nitrogen (NH_3) is known to promote Si nanocrystal formation via the dissociation of Si–H bonds [8,9]. The role of nitrogen and of atomic hydrogen can be investigated through the structural and optical analysis of the films.

In this work, the film properties were tuned by changing the NH_3 gas flow during deposition, and keeping the SiH_4 flow constant. In the following, we will refer to R , as the NH_3 versus SiH_4 gas flow ratio ($R = \text{NH}_3/\text{SiH}_4$). Fig. 1 shows the layer composition, in particular the atomic fractions of Si, N and H, determined by RBS and ERDA analysis.

In the as-deposited layers (Fig. 1a) the Si content reaches a maximum value for the lower amount of NH_3 gas ($R = 0.5$), then decreases to a minimum value for $R = 1.5$ and reaches a plateau when R increases further. On the other hand, the N content behaves in the opposite way since it exhibits a minimum value for $R = 0.5$, increasing up to a higher and constant value for $R > 1.5$.

The R values for which the Si and N contents are constant correspond to the stoichiometric composition of the layers, as confirmed by the refraction index (n) measurements. Indeed, for $R = 0.5$ the refractive index is very close to the typical n value of Si (3,85), and then it

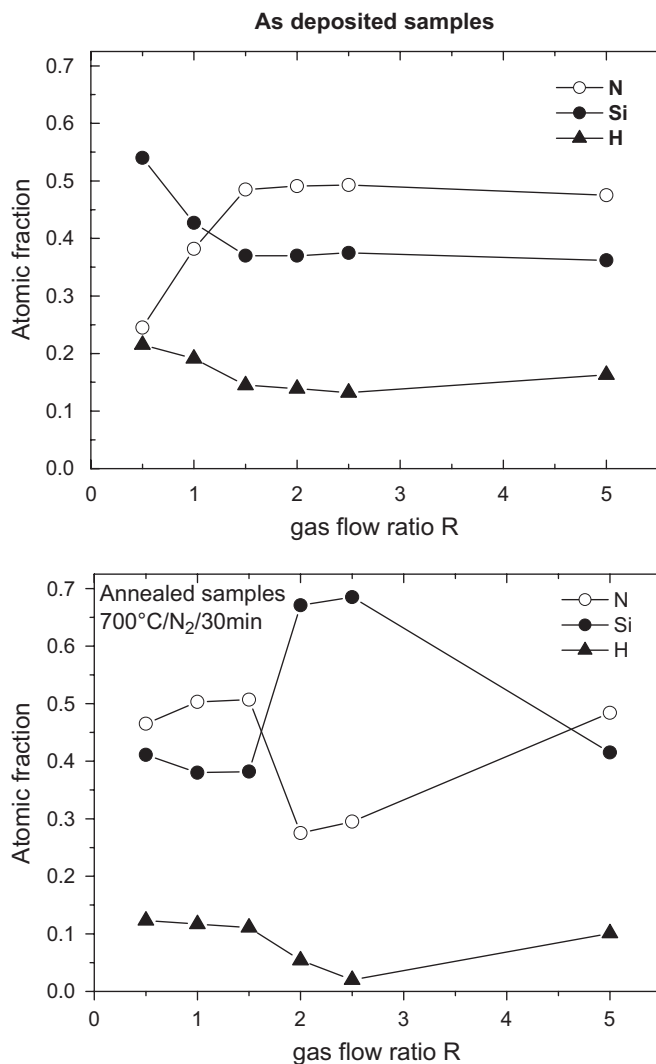


Fig. 1. Atomic fraction of Si, N and H vs. gas flow ratio measured by RBS and ERDA analysis: (a) as-deposited $\text{SiN}_x\text{:H}$ films and (b) after thermal annealing.

decreases towards the stoichiometric $\text{SiN}_x\text{:H}$ n value (1.9) for higher R ratios.

As for the hydrogen content in the amorphous $\text{SiN}_x\text{:H}$ layers, this is found to be maximum in the Si-rich film ($R = 0.5$) and to decrease slowly when R increases, up to a constant value of around 0.1.

The analysis of the samples after annealing (Fig. 1b) is more complicated. First of all, we can observe that the samples deposited with $R = 0.5$ and 1, which were Si-rich before annealing, becomes almost stoichiometric in composition. Indeed, we may assume that in the Si rich layers silicon atoms in excess combine with N_2 from the annealing atmosphere to form $\text{SiN}_x\text{:H}$. This behavior is facilitated by the high porosity of the layers (pore size ~ 8 nm), as observed by TEM (not shown here). The reaction will saturate when the composition is near to that of the stoichiometric one. Thus, for $R = 1.5$ we did not observe any variation in the Si and N atomic fraction before and after annealing. For R varying from 0.5 to 1.5, Si and N contents tend to stabilize at the same values of the as-deposited samples plateau region. Further studies are in progress concerning the annealing atmosphere, in order to better understand this behavior.

The data for $R = 2$ and 2.5 are quite particular. Indeed, films with these ratios exhibit strong silicon excess with respect to the stoichiometric composition, as confirmed by the refraction index increasing from 1.97 to 3.1 and from 1.6 to 2.97, respectively. For the annealed sample with $R = 5$ we only observe a slow increasing (decreasing) of the Si (N) concentration. Similarly to the behavior of the N content, the hydrogen concentration in the annealed samples is the lowest for the silicon-rich layers ($R = 2$ and 2.5). The hydrogen atomic content is in all cases lower for the annealed samples than for as-deposited ones, due to hydrogen exodiffusion and bonding arrangements.

These results are very important in our attempt to synthesize Si nanoparticles in a $\text{SiN}_x\text{:H}$ matrix, because the possibility of forming a very high Si excess in the matrix seems to be correlated to the atomic hydrogen content in the matrix. Indeed, it has been shown that a higher silicon concentration is found in the annealed films compared to that in as-deposited samples. Moreover, Si-rich as-deposited samples present a strong porosity which cannot completely disappear by the matrix rearrangement during annealing, whereas the Si-rich matrix after annealing did not exhibit any porosity after TEM observations.

To obtain more insight on the matrix composition evolution for different R and during annealing, we performed FTIR analysis, which provides fundamental information on the different bonds.

As the hydrogen content seems to affect the Si excess in the layers, we focused our attention in particular on the Si–H and N–H bonds.

Fig. 2(a) and (b) plots, respectively, the intensity of Si–H and N–H signal intensities normalized with respect to the Si–N signal amplitude. We can notice that for all R values, annealing the samples results in a decreasing of the

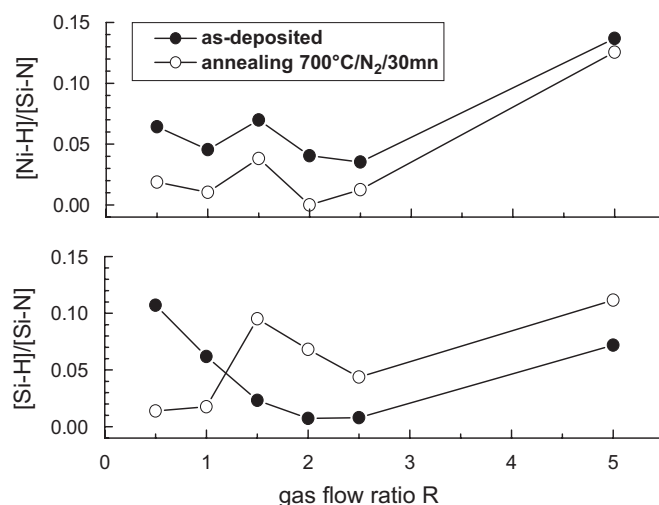


Fig. 2. Normalized [Si–H] and [N–H] FTIR absorption peak intensities as a function of gas flow ratio.

N–H bond concentration. As a consequence, atomic H can either become free to leave, in agreement with the decrease in the H concentration observed by ERDA, or saturate Si dangling bonds present in the matrix. On the other hand, for $R = 0.5$ and 1 the density of Si–H bonds decreases after annealing, due to the formation of Si–N bonds, due to additional nitrogen provided by the annealing atmosphere and to the large amount of Si excess within these samples, as has already been discussed. On the contrary, for $R \geq 1.5$ we observe a strong increase of the Si–H signal amplitude, suggesting that Si atoms with one or more dangling bond are present in large amounts in the matrix.

On the other hand, it can be noticed that a large amount of Si–H bonds means that there is a high concentration of the Si matrix that is not bound to N, which is in agreement with the results discussed above, and which can in principle give rise to Si cluster nucleation.

In order to elucidate this point and to investigate the possibility of forming Si clusters, we measured the PL spectra of the $\text{SiN}_x\text{:H}$ layers.

2.2. PL analysis

Figs. 3(a) and (b) show the PL spectra of as-deposited and annealed samples for R equal to 0.5 and 2, respectively. The choice of these ratios is based on their structural properties which reveal a silicon excess either before or after annealing. For $R = 0.5$, no room temperature PL is detected from the as-deposited sample. Although this sample presents a strong amount of excess Si, the film is highly porous and more likely it has a very disordered structure. In this case, the PL emission is quenched by the presence of a large amount of non-radiative recombination centers such as Si dangling bonds.

After annealing, this sample exhibits a strong PL emission, with a spectrum consisting of a weak peak

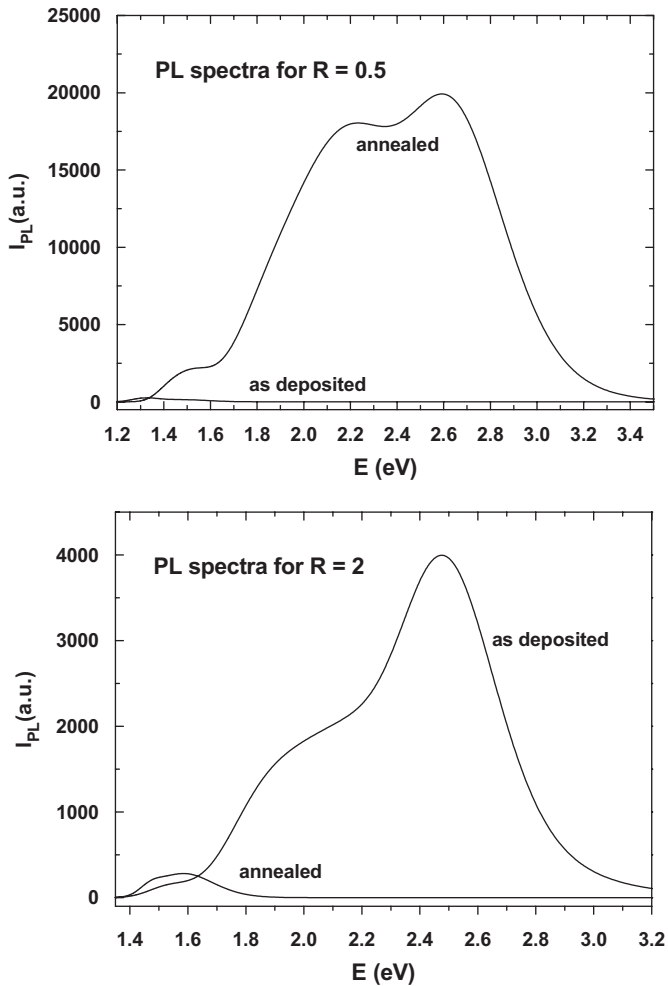


Fig. 3. Photoluminescence spectra of as-deposited and annealed $\text{SiN}_x\text{:H}$ films: (a) $R = 0.5$ and (b) $R = 2$.

centered around 1.5 eV and a very large contribution ranging from 1.8 to 3 eV that can be deconvoluted into 3 PL bands, centered at 2.7, 2.2 and 1.85 eV.

These bands have been extensively reported in the literature and are attributed by several authors [4,10–12] to nitrogen and silicon levels in the $\text{SiN}_x\text{:H}$ band gap. Based on the schematic representation used by Deshpande et al. [13], three types of traps participate in the PL in the $\text{SiN}_x\text{:H}$ matrix: Si dangling bonds (K° centers) that form a recombination center in the middle of the gap, and nitrogen defect states which are responsible for two levels within the gap, namely (N_4^+) close to the conduction band, and (N_2^0) close to the valence band. These defects give rise to large emission spectra because the optical gap varies depending on the film composition [14], which is not necessarily homogeneous in the film bulk [4,15].

Following this model, we may attribute the 1.8 eV peak to the recombination between the two nitrogen defects, the 2.2 eV peak to the Si dangling bonds, and the PL at the highest energy to the recombination either between the conduction band and the N_2^0 level, or between the level N_4^+ and the valence band. In any case, the presence of this large

band is related to a structural disorder in the matrix and to the presence of Si- and N-related defects.

On the contrary, the presence of the weak PL peak at 1.5 eV can be indicative of the Si excess in the matrix and then to the possibility of Si cluster formation. However, despite the highly Si-rich matrix observed for this sample ($R = 0.5$), no nanoparticles have been observed by TEM experiments.

Concerning the samples with $R = 2$, the as-deposited one shows a strong PL signal in the same energy range as for the $R = 0.5$ annealed sample. The analysis of the PL band shows that, except for a weak contribution at 1.5 eV, the spectra are composed again of three bands centered around 2.51, 2.2 and 1.85 eV, that can be related to the N and Si dangling bond as already discussed for the previous case.

For this particular sample, it is very interesting to follow the behavior of the PL emission before and after annealing. After annealing, all contributions from the defects vanish and quite a weak PL emission in the region around 1.5 eV is observed. From the structural analysis we have shown that such a sample exhibits Si excess in the matrix that can nucleate and form Si clusters. The PL emission detected at around 1.5 eV could be due to the presence of Si nanoparticles.

This assumption is corroborated by TEM analysis carried out on this sample. Fig. 4 shows the TEM cross-section image in defocused bright field conditions which revealed the presence of amorphous nanoparticles, with a diameter of around 3 nm.

It should be stated that in the previous case ($R = 0.5$, as deposited) the lack of observation of Si nanoparticles by

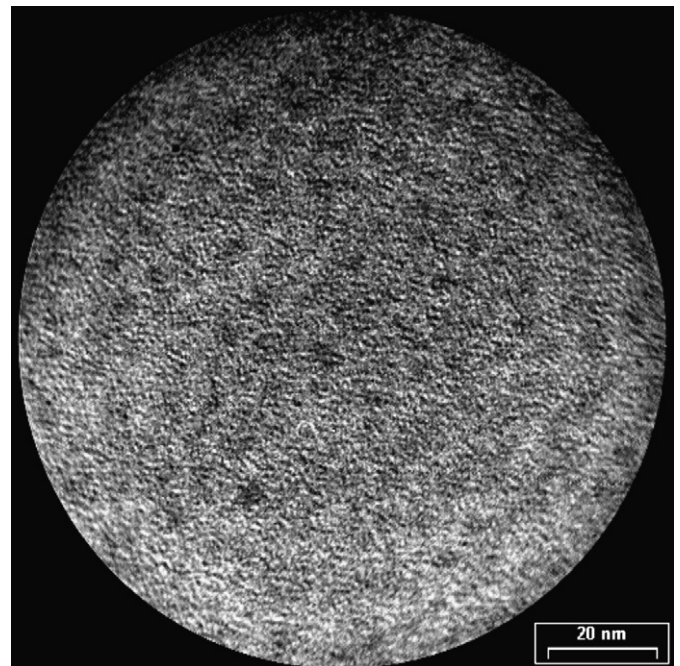


Fig. 4. Cross-sectional transmission electron microscopic image of silicon nanoparticles embedded in $\text{SiN}_x\text{:H}$ film deposited with gas flow ratio $R = 2$ and annealed at 700 °C during 30 min.

TEM is not sufficient to state that no nanoparticles have been formed, even if this is more likely the case. Indeed, if the nanoparticles size is too small, TEM observation in the bright field (BF) conditions is very difficult. On the other hand, as our particles are amorphous, it is impossible to image them in high resolution or in dark field (DF) conditions, as is usually carried out for Si nanocrystals in SiO₂ [16].

Defocused BF imaging is normally used to image systems of nanoparticles/matrix with a strong amplitude difference, such as in the case of Ge nanoparticles in SiO₂ [17]. Silicon amorphous nanoparticles in a SiN_x:H matrix have been imaged in these conditions by Park et al. [5]. But the possibility of observing depends very much on the contrast between the particles and the matrix, and consequently depends on the film stoichiometry. In the case of the as-deposited sample with $R = 0.5$ the matrix is strongly porous and full of structural defects and the conditions to observe possible nanocrystals if any are not fulfilled. Anyway, for this sample the most probable picture is that excess Si is not organized in nanoclusters but is part of the disordered matrix.

The same considerations for matrix quality and stoichiometry could be applied to the PL results. Indeed, the observed wide PL centered at around 1.5 eV does not correspond exactly to the emission energy of Si nanoparticles of 3 nm diameter which is expected to be about 1.9 eV. On the other hand, Kim et al. [7] reported amorphous silicon nanoparticles of 3–4 nm embedded in a SiN_x:H matrix that gives rise to PL at energies of 1.6–1.75 eV, quite close to our value. The difference might come from the composition of the matrix as well as from the efficiency of surface passivation of the silicon clusters. Indeed, it is well known that the PL emission in Si nanostructures is not only due to quantum confinement but is strongly dependent on surface states and passivation. In the case of Si nanocrystal embedded in SiO₂ for instance, when the crystallite size decreases to a few nanometers the difference (red shift) between the experimental data and quantum confinement prediction can be of almost 1 eV [18,19], and as large as 0.5 eV [20] if only one kind of surface defect is considered in the calculations [21]. In our case, post-annealing of the sample with $R = 2$ releases hydrogen from the N–H bonds. Part of the nitrogen atoms link to the silicon dangling bonds, forming new Si–N bonds and thus reducing the nitrogen defect density. In this situation it is possible that another part of the N atoms is released, in agreement with the stoichiometry change measured by RBS/ERDA. On the other hand, free hydrogen atoms either bond to silicon dangling bonds or passivate silicon nanoclusters present in the matrix upon deposition or formed during the annealing step. Such a situation results in a reduction of PL from the defects and an enhancement of PL from the silicon nanoparticles. Increasing the ratio $R (>2.5)$ leads to the formation of more nitrogen dangling bonds and a defect controlled PL. Similarly, reducing the ratio too much ($R < 0.5$) results in a

porous SiN_x:H film with a high density of silicon dangling bonds.

3. Conclusions

In this paper, we investigated the mechanisms involved in the synthesis of silicon nanoparticles in amorphous SiN_x:H films deposited by ECR-PECVD with different gas flow ratios R ($[\text{NH}_3]/[\text{SiH}_4]$) of NH₃ and SiH₄.

The formation of Si nanoparticles is related to excess Si in the matrix but good passivation conditions are necessary. In particular the optimization of the NH₃ gas flow is required. Indeed, depositing Si-rich films ($R \leq 0.5$) results in a porous SiN_x:H matrix with too high a density of silicon dangling bonds with no Si nanoparticle being observed by TEM. We have shown that the optimal situation is reached for the sample deposited with $R = 2$ after annealing, for which amorphous Si nanoparticles were detected by TEM observations. In such a situation we observed a reduction of PL from defects and an enhancement of PL from silicon nanoparticles. A higher concentration ($R > 2$) of NH₃ leads to the formation of more nitrogen dangling bonds and a defect controlled PL was measured.

Acknowledgments

The authors would like to thank J.J. Grob and J.P. Stoquert for the RBS and ERDA measurements. This work is partially funded by the European Commission through the Integrated project CRYSTALCLEAR, N°SES6-CT_2003-502583, and by Ministère de la Recherche Scientifique through the project ANR-PV-PHARE.

References

- [1] W.G.J.H.M. Van Sark, A. Meijerink, R.E.I. Schropp, J.A.M. Van Roosmalen, E.H. Lysen, Sol. Energy Mater. Sol. C 87 (2005) 395.
- [2] L.-Y. Chen, W.H. Chen, F. Chau-Nan Hong, Appl. Phys. Lett. 86 (2005) 193506.
- [3] Y.M. Wan, N. Buffet, K. Van der Jeugd, P. Mur, D. Mariolle, G. Nicotra, S. Lombardo, Solid-State Electron. 48 (2004) 1519.
- [4] V.A. Gritsenko, K.S. Zhuravlev, A.D. Milov, H. Wong, R.W.M. Kwok, J.B. Xu, Thin Solid Films 353 (1999) 20.
- [5] N.-M. Park, C.-J. Choi, T.-Y. Seong, S.-J. Park, Phys. Rev. Lett. 86 (2001) 1355.
- [6] M. Hirasawa, T. Orii, T. Seto, Appl. Phys. Lett. 88 (2006) 093119.
- [7] T.-Y. Kim, N.-M. Park, K.-H. Kim, G.Y. Sung, Y.-W. Ok, T.-Y. Seong, C.-J. Choi, Appl. Phys. Lett. 85 (2004) 5355.
- [8] T. Yasuda, D.S. Hwang, J.W. Park, K. Ikuta, S. Yamasaki, K. Tanaka, Appl. Phys. Lett. 74 (1999) 653.
- [9] N.-M. Park, S.H. Kim, G.Y. Sung, S.-J. Park, Chem. Vapor Depos. 8 (2002) 254.
- [10] V.V. Vasilev, I.P. Mikhailovskii, K.K. Svitashv, Phys. Stat. Sol. A 95 (1986) K37.
- [11] C. Savall, J.C. Bruyere, J. Krautwurm, J. Phys. D 28 (1995) 565.
- [12] K.S. Seol, T. Futami, T. Watanabe, Y. Ohki, M. Takiyama, J. Appl. Phys. 85 (1999) 6746.

- [13] S.V. Deshpande, E. Gulari, S.W. Brown, S.C. Rand, *J. Appl. Phys.* 77 (1995) 6534.
- [14] F. Giorgis, P. Mandracci, L. Dal Negro, C. Mazzoleni, L. Pavesi, *J. Non-Cryst. Solids* 266–269 (2000) 588.
- [15] V.A. Gritsenko, R.W.M. Kwok, Hei Wong and J. B. Xu., *J. Non-Cryst. Solids* 297 (2002) 96.
- [16] F. Iacona, G. Franzo, C. Spinella, *J. Appl. Phys.* 87 (2000) 1295.
- [17] C. Bonafos, B. Garrido, M. Lopez, A. Perez-Rodriguez, J.R. Morante, Y. Kihn, G. Ben Assayag, A. Claverie, *Appl. Phys. Lett.* 76 (2000) 3962.
- [18] J. von Behren, T. Van Buuren, M. Zacharias, E.H. Chimowitz, P.M. Fauchet, *Solid State Commun.* 105 (1998) 317.
- [19] S. Schuppler, S.L. Friedman, M.A. Marcus, D.L. Adler, Y.-H. Xie, F.M. Ross, J. Chabal, T.D. Harris, L.E. Brus, W.L. Brown, E.E. Chaban, P.F. Szajowski, S.B. Christman, P.H. Citrin, *Phys. Rev. B* 52 (1995) 4910.
- [20] M. Carrada, A. Wellner, V. Paillard, C. Bonafos, H. Coffin, A. Claverie, *Appl. Phys. Lett.* 87 (2005) 251911.
- [21] M.V. Wolkin, J. Jorne, P.M. Fauchet, *Phys. Rev. Lett.* 82 (1999) 197.